Published in final edited form as:
Nature. 2008 January 31; 451(7178): 591–595. doi:10.1038/nature06531.

Structure and Mechanism of the M2 Proton Channel of Influenza A Virus

Jason R. Schnell and **James J. Chou***
Department of Biological Chemistry and Molecular Pharmacology, Harvard Medical School, Boston, MA 02115, USA

Abstract

The integral membrane protein, M2, of influenza virus forms pH-gated proton channels in the viral lipid envelope[1]. The low pH of an endosome activates the M2 channel prior to hemagglutinin-mediated fusion. Conductance of protons acidifies the viral interior and thereby facilitates dissociation of the matrix protein from the viral nucleoproteins – a required process for unpacking of the viral genome[2]. In addition to its role in release of viral nucleoproteins, M2 in the trans-Golgi network (TGN) membrane prevents premature conformational rearrangement of newly synthesized hemagglutinin during transport to the cell surface by equilibrating the pH of the TGN with that of the host cell cytoplasm[3]. Inhibitng the proton conductance of M2 with the anti-viral drug amantadine or rimantadine inhibits viral replication[4–7]. We have determined by NMR the structure of the tetrameric M2 channel in complex with rimantadine. In the closed state, four tightly packed transmembrane (TM) helices define a narrow channel, in which a "tryptophan gate" is locked by inter-molecular interactions with aspartic acid. A C-terminal, amphipathic (AP) helix oriented nearly perpendicular to the TM helix, forms an inward facing base. Lowering the pH destabilizes the TM helical packing and unlocks the gate, admitting water to conduct protons, while the C-terminal base remains intact, preventing dissociation of the tetramer. Rimantadine binds at four equivalent sites near the gate on the lipid facing side of the channel and stabilizes the closed conformation of the pore. Drug-resistance mutations are predicted to counter the effect of drug binding by either increasing the hydrophilicity of the pore or weakening helix-helix packing, thus facilitating channel opening.

Keywords

influenza M2; proton channel; rimantadine binding; channel opening

M2 is a 97-residue single-pass membrane protein with its N- and C-termini directed toward the outside and inside of the virion, respectively; it is a homotetramer in its native state[8, 9]. The four TM helices form a channel in which His37 is the pH sensor and Trp41, the gate[6, 10, 11]. The adamantane-based drugs, amantadine and rimantadine, which target the M2 channel, have been used as first-choice antiviral drugs against community outbreaks of influenza A viruses for many years, but resistance to the adamantanes has recently become

*To whom correspondence may be addressed. james_chou@hms.harvard.edu.

Author contributions
J.R.S. and J.J.C. designed research, performed research, analyzed data, and wrote the paper.

Conflict of interest statement
J.J.C. and J.R.S. declare competing financial interests. A provisional patent entitled "Systems and Methods for Studying Influenza" was filed on October 25, 2007 on behalf of Harvard Medical School by Wolf, Greenfield & Sacks, P.C.

The structures have been deposited in the Protein Data Bank with accession code 2RLF.

widespread. Many structural models of this channel have been built, based on sequence analysis, mutagenesis, and solid-state NMR[8, 11, 12]. Many of these studies have been done on inherently unstable TM-only constructs, however, leading to conflicting structural conclusions.

While the TM-only peptide fails to form a stable tetramer, a construct of residues 18–60 [M2(18–60)], that includes 15 residues of the C-terminus in addition to the TM region, forms a stable tetramer in dihexanoyl-phosphatidyl-choline (DHPC) detergent micelles and yields high-resolution NMR spectra (Supplementary Fig. S1). In the closed conformation at pH 7.5, M2(18–60) is a homotetramer, in which each subunit has an unstructured N-terminus (residues 18–23), a channel-forming TM helix (residues 25–46), a short flexible loop (residues 47–50), and a C-terminal AP helix (residues 51–59). The TM helices assemble into a four-helix bundle with a left-handed twist angle of ~23° and a well-defined pore (Fig. 1). A ring of methyl groups from Val27 constricts the N-terminal end of the pore to ~3.1 Å (inner diameter). In agreement with proposed models[11, 13], His37 and Trp41 are inside the pore. A 3-bond, ^{15}N-^{13}Cγ scalar coupling ($^{3}J_{NC\gamma}$) value of 1.5 Hz (Supplementary Table 1), shows the His37 χ_1 rotamer to be predominantly *trans*, but with significant rotameric averaging. The χ_1 of Trp41 is essentially locked in the *trans* position, as determined by $^{3}J_{NC\gamma}$ of 2.6 Hz, while the χ_2 is also fixed at around −120° by the sidechain Hε1 – Nε1 dipolar coupling and NOEs. The Trp41 indole rings are at van der Waals (VDW) distance from each other, prohibiting passage of water or ions (Fig. 1c). The indole Hε1 of one subunit is on average 3.5 Å from the Asp44 carboxyl carbon of the adjacent subunit. The two residues can form an intermolecular hydrogen bond that stabilizes the closed Trp41 gate. The sidechain of Arg45 likely participates in an intermolecular interaction with Asp44. These findings are consistent with the increased pH-modulated activity of channels in which asparagine has replaced Asp44[14]. The C-terminal end of the channel extends into a loop (residues 47–50) that connects the TM domain to the C-terminal AP helix. RDCs and intra- and inter-monomer NOEs show that the AP helices lie roughly perpendicular (~82°) to the TM helices and assemble head-to-tail with a right-handed packing mode to form the base of the channel. The orientation and amphipathic character of the AP helices suggest that the C-terminal base lies on the surface of the membrane.

Residues 47–50 give no NOE peaks and have no stable, hydrogen-bonded structure in the detergent micelles used in our work. We believe that this segment adopts a more stable conformation in the viral membrane because Cys50, which we mutated to serine to avoid disulfide formation, is normally palmitoylated[15]. Modeling shows that extending the TM helix to Phe48 would place residue 50 facing the membrane, allowing for insertion of the palmitoyl acyl chain into the lipid bilayer. This minor rearrangement would also move the AP helices closer to the TM domain.

Drug binding has the effect of stabilizing the closed conformation. Upon addition of drug, the resonances of residues 43–46 at the C-terminus of the channel, which are severely exchange-broadened in the drug-free sample, became significantly sharper and more homogeneous (Supplementary Fig. S2). The protein-drug NOEs collected from four different NOESY spectra (Supplementary Fig. S3) place the binding site between adjacent helices at the C-terminal end of the TM domain near the Trp41 gate, on the membrane side of the channel (Fig. 1d). We could not detect drug NOEs in other parts of the protein, including the widely proposed drug-binding site in the pore of the channel. The amine head-group of rimantadine is in contact with the polar sidechains of Asp44, Arg45, and the indole amine of Trp41. The sidechains of Ile42 from one helix, and Leu40 and Leu43 from another helix form the hydrophobic walls of the binding pocket that interact with the adamantane group of rimantadine. Thus, rimantadine covers a unique polar patch in the otherwise hydrophobic environment of the TM domain. Interactions between rimantadine and the

channel are consistent with structure-activity relationships of the adamantane group[16]. In particular, the basic nitrogen group and size limits at the methyl site are critical. These requirements are the result of the interactions with Asp44 and the small hydrophobic pocket around Ile42, respectively.

Water NOEs measured in the 110 ms ^{15}N-separated NOESY experiments give a clear picture of water distribution relative to the channel (Fig. 2). The lipid-facing surface of the TM region is largely protected from water by the DHPC micelle. In the closed channel pore, the Val27 ring at the N-terminus and the Trp41 gate at the C-terminus essentially block water from freely diffusing into the pore from either side of the membrane. Within the TM region, only the amides of Ser31 and Ile32 have NOE crosspeaks at the chemical shift of water, probably corresponding to the hydroxyl proton of Ser31 in exchange with water. A polar residue is present at position 31 in all sequenced variants of M2, suggesting that proton conduction requires water bound to this site. This water may serve to bridge the proton relay from the N-terminal end of the pore to the His37 pH sensor. Water was detected at the C-terminus of the TM region, beginning at Arg45. The Hε1 of the Trp41 indole ring, which points toward the C-terminal side of the pore, also has a strong NOE to water, indicating that the base of the channel is accessible to bulk water.

Lowering the pH from 7.5 to 6.5 broadens most of the NMR resonances corresponding to the TM helix (Fig. 3a). The resonance broadening could not be attributed to protein aggregation, as the self-diffusion coefficients were essentially unchanged between pH 7.5 and 6.5. Thus, activation of the channel is coupled to increased conformational exchange in the TM domain. In contrast, the resonances of the AP helices are essentially unaffected by lowering the pH, indicating that the C-terminal base of the tetramer remains intact as the channel opens.

In addition to destabilizing helix-helix packing in the TM domain, channel activation must also correlate with increased dynamics of the Trp41 gate. Since the indole amide resonance of Trp41 remained intense as the pH was lowered from 7.5 to 6.0, it serves as a useful NMR probe for monitoring channel opening. We compared the ms timescale dynamics of the Trp41 indole ring between the closed and open states by carrying out relaxation-compensated Carr-Purcell-Meiboom-Gill (CPMG) experiments[17] at pH 7.5, 7.0, and 6.0. A two-site exchange model fits the dependence of ^{15}N relaxation due to chemical shift exchange on the frequency of refocusing ($1/\tau_{cp}$) of chemical shift evolution (Fig. 3b), implying that the gate switches between two configurations at any given pH. As the pH was lowered from 7.5 to 6.0, the rate of fluctuation increased by more than four-fold (Fig. 3b), indicating that channel activation “unlocks” the gate. Adding rimantadine to the channel at an intermediate pH of 7.0 slowed the timescale of the gate motion to nearly that of a drug-free gate at pH 7.5 (Fig. 3c). These results confirm that the reconstituted channels in the NMR sample are pH-gated, and are consistent with the location of the rimantadine site proximal to the gate.

The structure of the M2 proton channel thus reveals a simple yet effective gating. The tight packing of the four TM helices brings the bulky indole rings of Trp41 into VDW contact to form the channel gate. The gate is further stabilized by inter-subunit hydrogen bonds with Asp44. Lowering the pH protonates the imidazole rings of His37, destabilizing helix-helix packing by electrostatic repulsion. This conformational rearrangement breaks interactions between Trp41 and Asp44 and allows the gate to flip open. A pair of conserved N-terminal cysteines have been shown to form intermolecular disulfides in *vivo*[9]. Thus, the TM helices are tethered at one end by N-terminal disulfides and at the other end by the C-terminal base, ensuring that destabilization of the four-helix bundle during channel activation does not

cause dissociation of the tetramer (Fig. 4). Indeed, truncation of the AP helix results in channels that rapidly lose channel activity[18].

The external drug-binding site was unexpected. Drug-resistance mutations seemed to suggest a site inside the pore, because in early models of the channel, residues that lead to drug resistance were predicted to be pore-lining. The known mutations that confer drug resistance are L26F, V27A, A30T, S31N, G34E, and L38F. Mapping these residues onto the structure (Supplementary Fig. S7) reveals that Val27, Ala30, and Gly34 are pore-lining, but Leu26, Ser31 and Leu38 are in the helix-helix packing interface. Moreover, these mutations are spread out over more than three turns of the TM helix, covering a distance much larger than the dimensions of amantadine or rimantadine. Pinto and Lamb have pointed out that having a cork-plugging-the-bottle model is insufficient to explain all the results of electrophysiology studies[19]. For example, drug inhibition is more effective when applied to the closed channel than the open channel, which is not expected of a pore-blocking mechanism[5]. Several of the drug-resistance mutations in pore-lining residues have been shown to retain drug binding[20]. Although a pore blocker is expected to fit tightly in the pore, channel inhibition is unusually tolerant of modifications to the adamantane scaffold[16]. Together, the above observations suggest an allosteric inhibition mechanism.

Is the external binding site consistent with all drug-resistance mutations? Although the exact structural effects of resistance mutations are difficult to predict, what they do have in common is that they either perturb the helix-helix interface (L26F, V27A, S31N, L38F), or increase the hydrophilicity of the pore (A30T, G34E). From this observation, and from detection of a conformational exchange among multiple states at lowered pH, we propose an allosteric inhibition mechanism that can account for all of the mutations. In our model, drug binding makes the closed channel harder to open, while drug-resistance mutations destabilize the closed channel, making it easier to open. Replacing Val27 with alanine enlarges the N-terminal opening and weakens helix-helix packing, and therefore may facilitate channel opening. Ala30 and Gly34 are inside the pore, and replacing them with threonine and glutamate, respectively, may facilitate pore hydration, and in turn, channel opening. Leu26, Ser31 and Leu38 are helix-helix interface residues; their mutations likely perturb helix-helix packing and lower the energetic cost of channel opening.

Why then, are no drug-resistant mutations observed near the drug-binding site? In fact, few mutations are ever observed in this region of the channel (drug-resistant or otherwise), which is not surprising due to the functional constraints placed on these residues in proximity to the channel pH sensor (His37) and the channel gate (Trp41). As the structure illustrates, intermolecular contacts between Asp44 and Arg45 form an integral part of the channel gate, along with Trp41. The residues that form the hydrophobic walls of the binding pocket – Leu40, Ile42, and Leu43 – are on the lipid face of the channel and must retain hydrophobicity for membrane partitioning. In order to accommodate the Trp41 indole rings within the channel, the helices splay slightly at the C-terminus of the TM domain, and interhelical contacts below Leu38 – with the exception of the Trp41 sidechains – are no longer important for channel assembly. Thus, residues essential to channel assembly are in the N-terminal half of the TM helix, exactly where drug-resistance mutations occur.

Binding from the membrane side is consistent with the high membrane partition coefficient of adamantane drugs, which effectively concentrates them in the membrane and lowers their level in the aqueous phase[21, 22]. Adamantanes interact with a number of other ion channels, including viroporins from hepatitis C[23], the potassium channel Kcv of the chlorella virus PBCV-1[24], and the human NMDA receptors[25]. Hanatoxin, an allosteric inhibitor of voltage gated K^+ channels with a high membrane partition coefficient, also has an external binding site[26, 27]. Membrane-side binding may thus be a feature of many channel inhibitors. This

mode of inhibition could be advantageous for drug design because drug molecules are typically much larger than hydrated ions selected by ion channels, and therefore the energy barrier for drug to find a blocking site inside the channel pores would be much higher than targeting a functional site from the membrane side of the channel.

METHODS SUMMARY

The M2(18–60) polypeptide construct was expressed as a C-terminal fusion to trpLE with an N-terminal 9-His tag in the pMM-LR6 vector[28]. The M2(18–60)tetramer was reconstituted by dissolving peptide in solution containing 50 mM sodium phosphate, 6 M guanidine HCl, 150 mM DHPC, dialyzing against a solution containing 40 mM sodium phosphate (pH 7.5) and 30 mM glutamate, and concentrating. Rimantadine was added to the reconstituted protein. The final NMR sample used for structure determination contained 0.75 mM M2(18–60) (monomer), ~300 mM DHPC, and 40 mM rimantadine. Given the DHPC has an aggregation number of 27[29] and the strong partition coefficient of rimantadine in phospholipids (rimantadine aqueous solubility is very low, ~ 50 μM), locally, there are about 4 rimantadine molecules per micelle compartment in which the channel resides.

The NMR protocol employed was similar to that previously described by Oxenoid & Chou[30]. An extensive set of structural restraints including 230x4 intra- and 27x4 inter-molecular distance restraints derived from nuclear Overhauser enhancements (NOEs), 27x4 orientation restraints from residual dipolar couplings (RDCs), and 23x4 sidechain rotamers from 3-bond scalar couplings were used to generate an ensemble of 15 low energy structures with a backbone rmsd of 0.30 Å for the channel region, and 0.89 Å for all structured regions (Fig. 1a). The refinement statistics and NMR-derived restraints are summarized in Supplementary Table S1. Structure calculation was accomplished in two steps, in which the overall tetramer conformation was first defined by NOE-derived distance restraints and *J* coupling-derived dihedral restraints using a high-temperature simulated annealing protocol, and subsequently refined against RDCs at low temperature. More experimental details are given in the METHODS section below.

METHODS

Sample preparation

M2(18–60) was expressed into inclusion bodies as a fusion to $(His)_9$-trpLE[31]. The M2(18–60) peptide was released from the fusion protein by CNBr digestion in 70% formic acid (2 hr, 0.2 g/ml). The digest was dialyzed to water, lyophilized, and loaded onto a C4 column (Grace-Vydac) in 2:1:2 hexafluoroisopropanol:formic acid:water and separated on a gradient of 3:2 isopropanol:acetonitrile. The lyophilized peptide was refolded at 250 μM by dissolving in 6 M guanidine and 150 mM DHPC and dialyzing against the final NMR buffer containing 40 mM sodium phosphate and 30 mM glutamate. The sample was concentrated to a final M2(18–60) concentration of 0.75 mM (monomer). Rimantadine was added after concentrating. The concentration of DHPC was determined from ^{1}H NMR spectroscopy to be around 300 mM. Given the DHPC has an aggregation number of 27[29] and the strong partition coefficient of rimantadine in phospholipids (rimantadine aqueous solubility is very low, ~ 50 μM), locally, there are about 4 rimantadine molecules per micelle compartment in which the channel resides.

NMR spectroscopy

NMR experiments were conducted at 30°C on spectrometers equipped with cryogenic probes (Bruker, Billerica, MA). Sequence specific assignment of backbone $^1H^N$, ^{15}N, $^{13}C^\alpha$, and $^{13}C^\beta$ chemical shifts were accomplished using the TROSY versions of the HNCA and

HNCACB experiments on a ^{15}N-, ^{13}C, and 85% ^{2}H-labeled protein. Sidechain χ_1 and χ_2 rotamers were obtained from measurements of the 3-bond scalar couplings including $^{3}J_{NC\gamma}$, $^{3}J_{C'C\gamma}$ and $^{3}J_{C\alpha C\delta}$[32, 33]. ^{1}H-^{15}N RDCs were measured for the protein-detergent complex weakly aligned in radially-compressed polyacrylamide gel[34]. Intramonomer NOEs involving both backbone and sidechain protons were assigned using the 3D ^{15}N-edited and ^{13}C-edited NOESYs recorded with NOE mixing times of 110 and 150 ms, respectively, on a sample containing ^{15}N-, ^{13}C-labeled protein, rimantadine, and deuterated DHPC (D35-DHPC) (Avanti Polar Lipids, Inc.). For identifying contacts between adjacent monomers, intramonomer NOEs were first assigned to completion. This is possible owing to the low complexity of the NOESY spectra of M2(18–60) (see Supplementary Fig. S4&5). The remaining NOEs involving residues of the TM and AP helices, which could not be explained by intramonomer distances based on the known secondary structures, were identified to be intermonomer NOEs. The assignment of intermonomer distance restraints and structure calculation were carried out iteratively until all NOE crosspeaks in the NOESY spectra were self-consistent in the tetrameric structure. Protein-drug NOEs were first identified using the ^{15}N-edited and ^{13}C-edited NOESYs described above, and subsequently confirmed by a ^{15}N-edited NOESY recorded with 500 ms mixing time on a sample containing uniform ^{15}N- and ^{2}H-labeled protein, rimantadine, and D35-DHPC.

Structure determination

Structures were calculated using the program XPLOR-NIH[35]. The secondary structure of the monomer was first calculated from random coil using intramonomer NOEs, backbone dihedral restraints derived from chemical shifts (TALOS)[36], and side chain χ_1 and χ_2 restraints shown in Supplementary Table 2. A total of 20 monomer structures were calculated using a standard high-temperature simulated annealing (SA) protocol in which the bath temperature was cooled from 1000 to 200 K. To obtain an initial set of tetramer structures, four copies of the lowest-energy monomer structure calculated above were used. The same high-temperature SA run was performed in the presence of intermonomer NOEs and all other intramonomer restraints except RDCs. For each experimental intermonomer NOE between two adjacent subunits, four identical distance restraints were assigned respectively to all pairs of neighboring subunits to satisfy the condition of C4 rotational symmetry. During the annealing run, the bath is cooled from 1000 to 200 K with a temperature step of 20 K, and 6.7 ps of Verlet dynamics at each temperature step, using a time step of 3 fs. A total of 100 tetramer structures were calculated, and independently cross validated by ^{1}H-^{15}N RDCs. Fitting of RDCs to structures was done by singular value decomposition (SVD), using the program PALES[37]. The goodness of fit was assessed by Pearson correlation coefficient (r) and quality factor (Q). Among the 100 structural models, 15 structures of which the individual subunits have on average the best agreement with RDCs (r ~ 0.91 and Q ~ 0.25) were selected for a final, low-temperature refinement against RDCs in the presence of all NOE and dihedral restraints. During the refinement, the bath was cooled from 200 to 20 K with a temperature step of 10 K, and 6.7 ps of Verlet dynamics at each temperature step, using a time step of 3 fs. The force constants for NOE and experimental dihedral restraints were fixed at 100 kcal mol^{-1} Å^{-2} and 40 kcal mol^{-1} rad^{-2}, respectively. RDC restraint force constant was ramped from 0.01 to 0.125 kcal mol^{-1} Hz^{-2}. The force constant for RDCs was set to a small value to prevent violation of NOE restraints. For each of the 15 structures validated by RDCs, 10 RDC-refined structures were generated. From that set, the structure with the lowest total energy was added to the final ensemble to describe the structural diversity of the solution structure. The structure with heavy atom conformation closest to the mean was chosen to represent the final ensemble. Without violating any NOE restraints, the final subunit structures fit RDCs to r of 0.98 and Q of 0.15, with D_a = 14.2 Hz and R_h = 0.24. Final backbone RMSD from the mean in the TM and AP

domains were 0.30 Å and 0.56 Å, respectively. The structures have been deposited in the Protein Data Bank with accession code 2RLF.

Measurement of chemical exchange in the Trp41 indole ring

The timescale of chemical shift exchange of the Trp41 sidechain was measured using a relaxation-compensated CPMG experiment[17] in 1D mode at ^{1}H frequency of 600 MHz. The dependence of ^{15}N relaxation due to chemical exchange on the frequency of refocusing ($1/\tau_{cp}$) of chemical shift evolution was fitted to a two-site exchange model given by $R_{ex} \propto 1-(2\tau_{ex}/\tau_{cp})\tanh(\tau_{cp}/2\tau_{ex})$, where R_{ex} is the contribution to transverse relaxation due to chemical shift exchange, and τ_{ex} is the correlation time of the process that is generating the chemical shift exchange[38].

Supplementary Material

Refer to Web version on PubMed Central for supplementary material.

Acknowledgments

We thank Marcelo Berardi for many discussions and Stephen Harrison for assisting with the manuscript. This work was supported by NIH grant AI067438 and the Pew Scholars Program in the Biomedical Sciences awarded to J.J.C. J.R.S is supported by an NIH F32 postdoctoral fellowship.

References

1. Lamb, RA.; Holsinger, LJ.; Pinto, LH. Receptor-Mediated Virus Entry into Cells. Wimmer, E., editor. Cold Spring Harbor Laboratory Press; Cold Spring Harbor, NY: 1994.
2. Helenius A. Unpacking the Incoming Influenza-Virus. Cell. 1992; 69:577–578. [PubMed: 1375129]
3. Ciampor F, et al. Evidence that the amantadine-induced, M2-mediated conversion of influenza A virus hemagglutinin to the low pH conformation occurs in an acidic trans Golgi compartment. Virology. 1992; 188:14–24. [PubMed: 1566569]
4. Hay AJ, Wolstenholme AJ, Skehel JJ, Smith MH. The molecular basis of the specific anti-influenza action of amantadine. EMBO J. 1985; 4:3021–3024. [PubMed: 4065098]
5. Wang C, Takeuchi K, Pinto LH, Lamb RA. Ion channel activity of influenza A virus M2 protein: characterization of the amantadine block. J Virol. 1993; 67:5585–5594. [PubMed: 7688826]
6. Pinto LH, Holsinger LJ, Lamb RA. Influenza virus M2 protein has ion channel activity. Cell. 1992; 69:517–528. [PubMed: 1374685]
7. Chizhmakov IV, Geraghty FM, Ogden DC, Hayhurst A, Antoniou M, Hay AJ. Selective proton permeability and pH regulation of the influenza virus M2 channel expressed in mouse erythroleukaemia cells. J Physiol (London). 1996; 494:329–336. [PubMed: 8841994]
8. Sugrue RJ, Hay AJ. Structural characteristics of the M2 protein of influenza A viruses: evidence that it forms a tetrameric channel. Virology. 1991; 180:617–624. [PubMed: 1989386]
9. Holsinger LJ, Lamb RA. Influenza Virus M2 Integral Membrane Protein is a Homotetramer Stabilized by Formation of Disulfide Bonds. Virology. 1991; 183:32–43. [PubMed: 2053285]
10. Tang Y, Zaitseva F, Lamb RA, Pinto LH. The gate of the influenza virus M2 proton channel is formed by a single tryptophan residue. J Biol Chem. 2002; 277:39880–39886. [PubMed: 12183461]
11. Pinto LH, et al. A functionally defined model for the M2 proton channel of influenza A virus suggests a mechanism for its ion selectivity. Proc Natl Acad Sci USA. 1997; 94:11301–11306. [PubMed: 9326604]
12. Wang JF, Kim S, Kovacs F, Cross TA. Structure of the transmembrane region of the M2 protein H + channel. Protein Science. 2001; 10:2241–2250. [PubMed: 11604531]
13. Kukol A, Adams PD, Rice LM, Brunger AT, Arkin IT. Experimentally based orientational refinement of membrane protein models: A structure for the Influenza A M2 H+ channel. J Mol Biol. 1999; 286:951–962. [PubMed: 10024461]

14. Betakova T, Ciampor F, Hay AJ. Influence of residue 44 on the activity of the M2 proton channel of influenza A virus. J Gen Virol. 2005; 86:181–4. [PubMed: 15604445]
15. Sugrue RJ, Belshe RB, Hay AJ. Palmitoylation of the influenza A virus M2 protein. Virology. 1990; 179:51–56. [PubMed: 2219738]
16. Aldrich PE, et al. Antiviral agents. 2. Structure-activity relationships of compounds related to 1-adamantanamine. J Med Chem. 1971; 14:535–43. [PubMed: 5091970]
17. Loria JP, Rance M, Palmer AG. A relaxation-compensated Carr-Purcell-Meiboom-Gill sequence for characterizing chemical exchange by NMR spectroscopy. Journal of the American Chemical Society. 1999; 121:2331–2332.
18. Tobler K, Kelly ML, Pinto LH, Lamb RA. Effect of cytoplasmic tail truncations on the activity of the M(2) ion channel of influenza A virus. J Virol. 1999; 73:9695–701. [PubMed: 10559278]
19. Pinto LH, Lamb RA. Understanding the mechanism of action of the anti-influenza virus drug amantadine. Trends Microbiol. 1995; 3:271. [PubMed: 7551640]
20. Astrahan P, Kass I, Cooper MA, Arkin IT. A novel method of resistance for influenza against a channel-blocking antiviral drug. Proteins. 2004; 55:251–7. [PubMed: 15048819]
21. Subczynski WK, Wojas J, Pezeshk V, Pezeshk A. Partitioning and Localization of Spin-Labeled Amantadine in Lipid Bilayers: An EPR Study. J Pharm Sci. 1998; 87:1249–1254. [PubMed: 9758685]
22. Wang JF, Schnell JR, Chou JJ. Amantadine partition and localization in phospholipids membrane: a solution NMR study. Biochem Biophys Research Comm. 2004; 324:212–217. [PubMed: 15465004]
23. Griffin SD, Beales LP, Clarke DS, Worsfold O, Evans SD, Jaeger J, Harris MP, Rowlands DJ. The p7 protein of hepatitis C virus forms an ion channel that is blocked by the antiviral drug, Amantadine. FEBS Lett. 2003; 535:34–38. [PubMed: 12560074]
24. Plugge B, et al. A potassium channel protein encoded by chlorella virus PBCV-1. Science. 2000; 287:1641–4. [PubMed: 10698737]
25. Svensson TH. Dopamine release and direct dopamine receptor activation in the central nervous system by D-145, an amantadine derivative. Eur J Pharmacol. 1973; 23:232–8. [PubMed: 4746740]
26. Swartz KJ, MacKinnon R. Hanatoxin Modifies the Gating of a Voltage-Dependent K+ Channel through Multiple Binding Sites. Neuron. 1997; 18:665–73. [PubMed: 9136774]
27. Lee SY, MacKinnon R. A membrane-access mechanism of ion channel inhibition by voltage sensor toxins from spider venom. Nature. 2004; 430:232–5. [PubMed: 15241419]
28. Call ME, et al. The structure of the zetazeta transmembrane dimer reveals features essential for its assembly with the T cell receptor. Cell. 2006; 127:355–68. [PubMed: 17055436]
29. Chou JJ, Baber JL, Bax A. Characterization of phospholipids mixed micelles by translational diffusion. J Biomol NMR. 2004; 29:299–308. [PubMed: 15213428]
30. Oxenoid K, Chou JJ. The structure of phospholamban pentamer reveals a channel-like architecture in membranes. Proc Natl Acad Sci U S A. 2005; 102:10870–5. [PubMed: 16043693]
31. Blacklow SC, Kim PS. Protein folding and calcium binding defects arising from familial hypercholesterolemia mutations of the LDL receptor. Nat Struct Biol. 1996; 3:758–762. [PubMed: 8784348]
32. Bax A, et al. Measurement of homo- and heteronuclear J couplings from quantitative J correlation. Methods Enzymol. 1994; 239:79–105. [PubMed: 7830604]
33. MacKenzie KR, Prestegard JH, Engelman DM. Leucine side-chain rotamers in a glycophorin A transmembrane peptide as revealed by three-bond carbon-carbon couplings and 13C chemical shifts. J Biomol NMR. 1996; 7:256–260. [PubMed: 8785502]
34. Chou JJ, Gaemers S, Howder B, Louis JM, Bax A. A simple apparatus for generating stretched polyacrylamide gels, yielding uniform alignment of proteins and detergent micelles. J Biomol NMR. 2001; 21:377–382. [PubMed: 11824758]
35. Schwieters CD, Kuszewski J, Tjandra N, Clore GM. The Xplor-NIH NMR molecular structure determination package. J Magn Reson. 2002; 160:66–74.

36. Cornilescu G, Delaglio F, Bax A. Protein backbone angle restraints from searching a database for chemical shift and sequence homology. J Biomol NMR. 1999; 13:289–302. [PubMed: 10212987]
37. Zweckstetter M, Bax A. Prediction of sterically induced alignment in a dilute liquid crystalline phase: aid to protein structure determination by NMR. J Am Chem Soc. 2000; 122:3791–3792.
38. Allerhand A, Thiele E. Analysis of Carr-Purcell Spin-Echo NMR Experiments on Multiple-Spin Systems. II. The Effect of Chemical Exchange. J Chem Phys. 1966; 45:902–916.

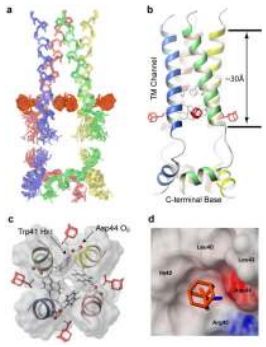

Figure 1.

Structure of the M2 channel. **a,** An ensemble of 15 low energy structures derived from NMR restraints. Since residues 47–50 are unstructured, the TM helices (residues 25–46) and the AP helices (residues 51–59) are superimposed separately. The backbone rmsd for the TM and AP helices are 0.30 Å and 0.56 Å, respectively. **b,** A ribbon representation of a typical structure from the ensemble in **a**, showing the left-handed packing of the TM helices, right-handed packing of the AP helices, the sidechains of His37 and Trp41, as well as the drug rimantadine (colored in red). **c,** A close-up view from the C-terminal side of the channel showing the Trp41 gate and how it is stabilized by the inter-monomer hydrogen bond between Trp41 Hε1 of one TM helix and Asp44 carboxyl of the adjacent TM helix. **d,** The surface representation of the rimantadine binding pocket, showing the Asp44, the indole amine of Trp41, and Arg45 that form the polar patch, as well as the hydrophobic wall composed of Leu40, Ile42, and Leu43.

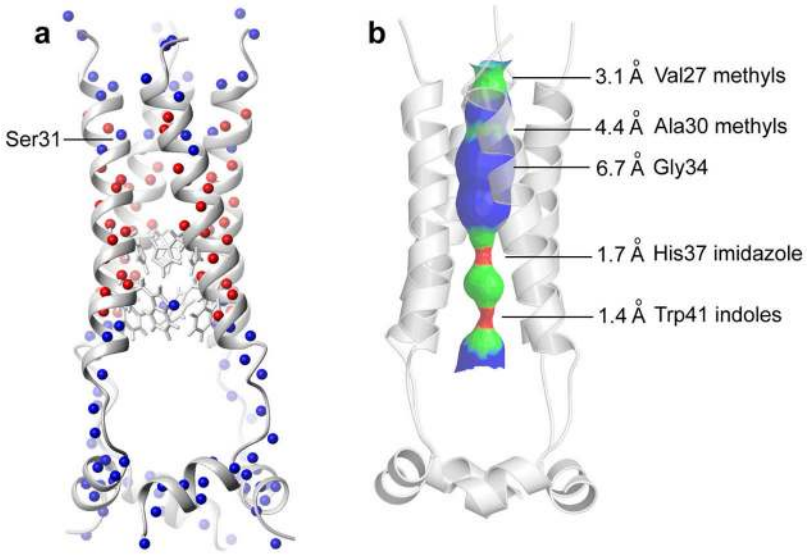

Figure 2.

Water accessibility of the M2 channel. **a,** Distribution of water NOEs relative to the structure. Amide protons colored in blue have a NOE crosspeak to water. Those that do not are colored red. **b,** The pore surface calculated using the program HOLE. The region of the channel colored in green is only wide enough to allow passing of a water molecule, where as the blue portion can accommodate two or more water molecules.

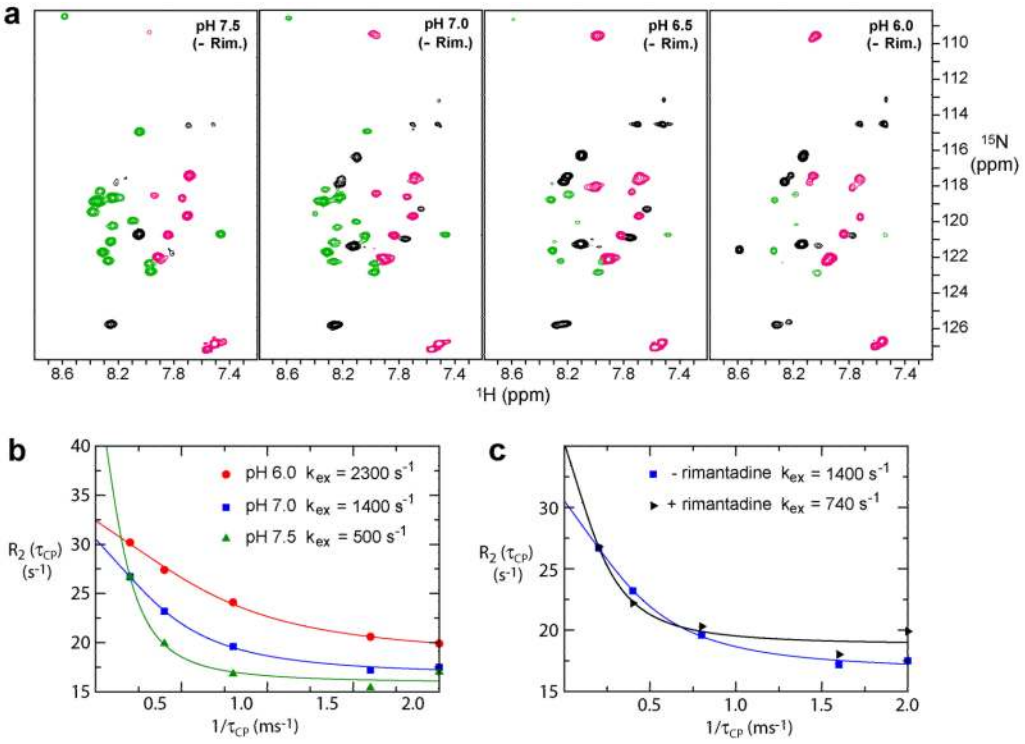

Figure 3.

Low-pH induced destabilization of the channel and opening of the Trp41 gate. **a,** ^{1}H-^{15}N TROSY spectra of reconstituted M2(18–60) tetramer at pH 6.0, 6.5, 7.0, and 7.5, in the absence of rimantadine, recorded at 500 MHz ^{1}H frequency and 30 °C. The coloring of the peaks is: green – TM helix; pink – AP helix; black – N-terminal loop. **b,** The ^{15}N R_2 (pure $R_2 + R_{ex}$) of the Trp41 Nε1 as a function of the frequency of refocusing ($1/\tau_{cp}$) of chemical shift evolution obtained at pH 7.5, 7.0, and 6.0, showing faster timescale motion of the Trp41 gate as the channel is activated. **c,** Comparsion between $R_2(\tau_{cp})$ at pH 7.0 in the absence (blue) and presence (black) of rimantadine, demonstrating that the drug slows down the gate flipping at this pH.

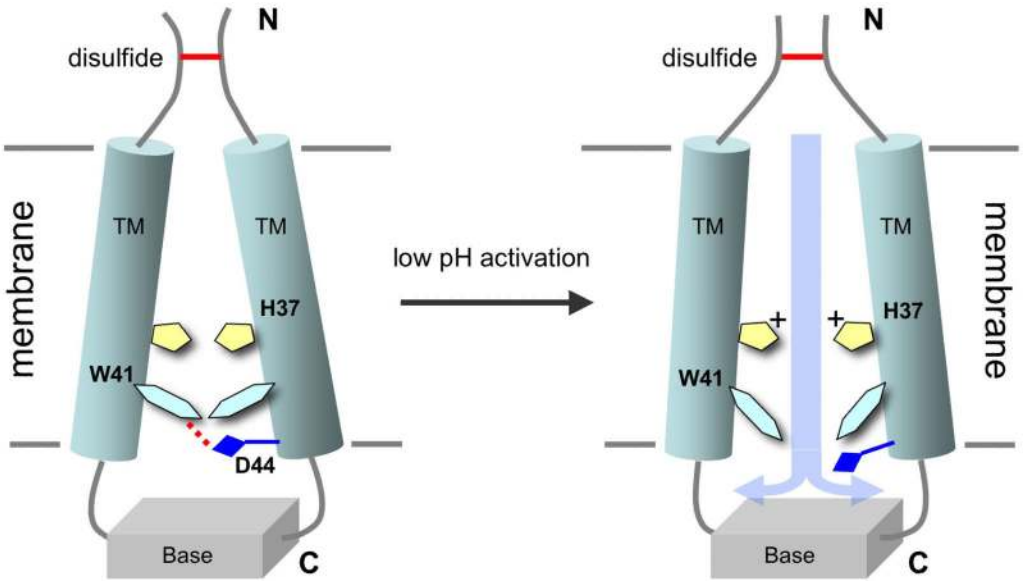

Figure 4.

Schematic illustration of M2 channel activation. At high pH, the TM helices are packed tightly and the tryptophan gate is locked through intermolecular interactions with Asp44. At low pH, protonation of the His37 imidazoles destabilizes the TM helix packing, allowing hydration of the channel pore, and proton conductance. The C-terminal base of the tetramer and N-terminal disulfide bonds keep the channel from completely disassembling. For clarity, only two of the four monomers are shown.